PUBLICATIONS OF THE ASTRONOMICAL SOCIETY OF THE PACIFIC
97:551–559, June 1985

RADIAL VELOCITIES OF RR LYRAE STARS

SUZANNE L. HAWLEY AND THOMAS G. BARNES III
Department of Astronomy and McDonald Observatory, RLM 15.308, University of Texas, Austin, Texas 78712
Received 1985 February 2

We obtained 283 spectra of 57 RR Lyrae stars using the 2.1-m telescope at McDonald Observatory. Radial velocities were determined using a software cross-correlation technique. New mean radial velocities were determined for 46 of the stars.

Key words: radial velocities—stars: RR Lyrae—variable stars (general)

I. Introduction

Radial velocities of field RR Lyrae stars are essential to statistical parallax analyses such as that of Hemenway (1975). In this kind of analysis radial velocities are combined with proper motion and position information to determine, in a statistical manner, the kinematic properties and absolute magnitude of a sample of stars. When applied to the field RR Lyrae stars, this method is an important tool for probing the kinematics of the Galactic halo. It also provides a firm basis for the use of RR Lyrae variables as primary distance indicators. However, as Stothers (1983) notes, absolute magnitudes from the statistical parallax method are currently unreliable due to the discrepant results obtained by various authors. We intend to repeat the analysis using a rigorous mathematical approach and an improved data set. To lay the groundwork for that project, we have first sought to improve the mean radial-velocity determinations for many of the stars.

The field RR Lyrae stars used in statistical studies often have mean radial velocities based on only one or two observations. Assumed epochs and periods are then used to locate the velocities on a standard radial-velocity curve. Since the radial-velocity amplitude of the pulsation is typically 50–70 km $\sec^{-1}$, the accuracy of the mean velocity can be greatly improved by observing the star several times during the pulsation cycle. The standard radial-velocity curve can then be fit to the data to determine the mean velocity, without relying on a published epoch (often 40 years out of date!).

We have obtained radial velocities for 57 RR Lyrae variables which permit improvement of the mean radial velocities for 46 of them. These will be combined with other radial velocities and new proper motions (Wan, Mao, and Ji 1980) in a statistical analysis of RR Lyrae absolute magnitudes and kinematics in a later paper (Hawley et al. 1985).

II. Observations

The observations were made using a Cassegrain spectrograph on the 2.1-m telescope at McDonald Observatory. A Reticon detector was used on 1982 September 14 UT and 1982 October 25–31 UT, and a CCD detector on 1983 January 22–29 UT, May 2–8 UT, June 27–30 UT, and July 1–4 UT. The Reticon detector is a bare, cooled, self-scanned device which has been described previously by Vogt, Tull, and Kelton (1978). It employs two Reticon arrays each 936 diodes in length and has a readout noise of about 1000 electrons per diode. It has been used extensively in radial-velocity studies of catalysmic variables by Hessman et al. (1984). We have used their cross-correlation method in our analysis.

The CCD detector is a thinned, cooled, back-illuminated RCA chip with 512 × 320 diodes and a readout noise of about 60 electrons per diode. To make the CCD data compatible with the Reticon data-reduction programs, the CCD was used in a Reticon simulation mode. In this mode, the spectra fall along the "512" direction on two effective "arrays," each 5 diodes wide, and spaced roughly 10 diodes apart. The 5 diodes, which are perpendicular to the dispersion, are then coadded in the data acquisition software to produce two 512 × 1 spectra. These may be reduced in the same manner as the two 936 × 1 spectra obtained from the Reticon. The dispersion, set by the grating, was 1.75 Å diode^{-1}. Thus the Reticon spectra cover the region from roughly 3600 Å–5000 Å while the CCD spectra extend from 3600 Å–4500 Å.

The observing procedure was the same as that described in detail in Stover, Robinson, Nather, and Montemayor (1980) (hereafter SRNM). Briefly, the spectrograph has two one-arc-second entrance slits; for a given observation, the star spectrum is recorded through one slit and the night-sky spectrum through the other. The star is then moved to the second slit and another exposure is taken. By subtracting the night-sky spectrum from the star spectrum taken in the same slit, both sky and background dark signal are removed. This procedure also has the advantage of providing two independent stellar spectra, taken a few minutes apart. Argon and neon lamps for wavelength calibration were observed before and after each pair of stellar spectra. A tungsten filament lamp was also observed to determine the small scale detector response. Finally, several radial-velocity standard stars were observed each night to set the radial-velocity scale and to define the mask for the software cross-correlation.

The data were reduced in the following manner. First, small-scale sensitivity variations in individual diodes on the detector were removed using the tungsten lamp spectra and standard flat-fielding techniques. Typically these corrections were of the order of 1%. Wavelength calibrations were determined before and after each pair of stellar spectra using the argon and neon lamp spectra. These calibrations were then interpolated to obtain the wavelength calibration appropriate to the midpoint of each stellar observation. A linear fit of wavelength to diode was found to be adequate for the CCD spectra while the Reticon data required a third-order polynomial fit. The spectra were then transformed to a logarithmic wavelength scale, as discussed in detail in SRNM, and heliocentric velocity corrections were applied.

We did not correct for the low frequency response by putting the spectra on a standard flux scale. Because the detectors both have better response in the red, the spectra have much better signal-to-noise ratio in the longer wavelength region. If we were to correct for the low-frequency instrumental response, it would artificially elevate the blue continuum, so that absorption features in the noisy, short-wavelength region would be given a larger weight in the cross-correlation fit. By using the uncorrected spectra, the depth of an absorption feature is determined by the local continuum and hence features are effectively weighted by the amount of signal in the spectrum at the wavelength of the feature.

The standard stars, chosen from the Astronomical Almanac compilation of standard radial-velocity stars, were the earliest spectral type available (typically late-F or early-G stars). These are of later spectral type than the RR Lyrae stars, which range from early A to late F. However, studies of radial-velocity meter data (e.g., Fletcher et al. 1982) indicate that the effective cross-correlation velocity is not affected by the spectral type of the mask from type F0 to M6.

A software cross-correlation mask was formed from the standard-star spectra. The standards were shifted from their known radial velocities to zero velocity and summed to form the mask. The strong absorption lines from the hydrogen Balmer series and Ca II H and K were masked out, since it is well known that these broad, saturated lines do not track the photospheric radial velocity (Preston and Paczynski 1964). The stellar spectra were then cross-correlated against the mask and a Gaussian was fit to the resulting cross-correlation function. The location of the Gaussian peak measures the radial velocity of the star relative to the zero velocity mask.

The standard-star spectra from each observing run were also cross-correlated with the mask to check for any systematic effects. Only one such effect was found. Table I shows the mean and standard deviation of the standard-star observations taken during a given observing run in a given slit. Ideally, the means should all equal zero. Significant differences in the values between the two slits were found in the May and June–July observing runs. These probably indicate that the centroid of the star image was sytematically displaced in one slit relative to the other, probably by a slight misalignment of the spectrograph optics. This effect would not be visible to the observer since only one-tenth arc second displacement is needed to account for the worst case. It was straightforward to correct for this small effect; the value needed to make the mean in a slit equal to zero was added to all of the stellar spectra taken in that slit during a particular observing run. Thus, for example, all of the spectra taken in slit 1 during the May 1983 CCD run had 7.64 km sec^{-1} added to their cross-correlation velocities.

The last column in Table I shows the standard deviation from the corrected standard-star spectra for each observing run. We find an uncertainty of about $\pm$ 12 km sec^{-1} for the CCD data. The Reticon gave much more accurate results than the CCD for the bright standard stars, but its signal-to-noise ratio in the RR Lyrae spectra was generally lower than that for the CCD. Thus it is appropriate to take the same uncertainty of $\pm$ 12 km sec^{-1} for all of the individual observations.

III. Data

The RR Lyrae spectra were cross-correlated against the standard-star mask, corrected to the heliocentric radial velocity at the midpoint of the observation, and corrected for the slit misalignment (if appropriate) to obtain the final

TABLE I

Comparison of Radial Velocities from Slits 1 and 2

Observing Run	No. of Obs. Slit 1	No. of Obs. Slit 2	Mean Velocity Slit 1	Mean Velocity Slit 2	Std. Dev. Slit 1	Std. Dev. Slit 2	Final Std. Dev.
Reticon, Sept,Oct 1982	15	15	-0.05	-1.04	3.00	4.47	3.74
CCD, January 1983	19	18	0.09	-0.54	13.22	13.70	13.27
CCD, May 1983	13	13	-7.64	0.71	11.54	12.39	11.70
CCD, June-July 1983	20	19	-3.53	1.33	11.39	10.46	10.85

radial velocity. These velocities are given in Table II, along with the Heliocentric Julian Date (HJD) at the midpoint of the observation and the phase, computed from the most recent epoch and period found in the GCVS. (The phases computed from these epochs and periods are in many cases inappropriate to the modern epoch. Thus, the phases shown in Table II should only be used to discern the relative phasing of the radial velocities.) Uncertain values are indicated by a colon.

Table II also includes a few observations made with the radial-velocity meter at the coudé focus of the 2.1-m

TABLE II

RR Lyrae Radial Velocity Results

HJD (2440000+)	V_r (km/sec)	PHASE	
AC AND	(2432467.373,	0.52512677)	
5226.867	-26	0.93	
5226.888	-23	0.97	
5269.725	-51	0.55	
5269.7365	-44	0.57	
AT AND	(2429146.374,	0.6169136)	
5269.680	-227	0.44	
5269.6915	-228	0.45	
AA AQL	(2424347.397,	0.36178688)	
5273.595	-61	0.23	
5273.616	-66	0.29	
5515.9085	-18	0.00	
5515.9225	-37	0.04	
5517.864	-35	0.40	
5517.8795	-21:	0.45	
5518.9055	-47	0.28	
5518.9205	-40	0.33	
5520.875	-13	0.73	
5520.890	-8:	0.77	
V341 AQL	(2434240.348,	0.57802018)	
5272.617	-103	0.30	
5272.634	-79	0.33	
5515.9415	-95	0.27	
5515.954	-91	0.29	
5517.9035	-54	0.66	
5517.9185	-51	0.69	
5519.874	-105	0.07	
5519.882	-119	0.08	
SX AQR	(2439796.326,	0.535712)	
5273.657	-159	0.35	
5273.678	-152	0.39	
X ARI	(2439059.056,	0.651152)	
5226.976	-29	0.32	
5226.9865	-17	0.34	

TABLE II (Continued)

HJD (2440000+)	V_r (km/sec)	PHASE	
TZ AUR	(2419902.432,	0.391674615)	
5358.7075	63	0.43	
5358.7215	69	0.46	
5359.732	23	0.04	
5359.746	21	0.08	
ST BOO	(2419181.486,	0.622290687)	
5449.865	-11	0.40	(rvm)
5458.8005	27	0.75	
5458.816	34	0.78	
5460.8475	47	0.04	
5460.860	8	0.06	
5515.754	-12	0.27	
5515.7665	-10	0.29	
5517.7285	15	0.45	
5517.744	9:	0.47	
TV BOO	(2441097.345,	0.3125594)	
5457.817	-56	0.86	
5457.8345	-26	0.91	
5459.850	-98	0.36	
5459.864	-92	0.41	
5461.824	-71	0.68	
5461.838	-40	0.72	
5515.7075	-39	0.07	
5515.7215	-42	0.12	
TW BOO	(2426891.268,	0.53227315)	
5460.8145	-111	0.25	
5460.8285	-115	0.28	
5514.694	-87	0.48	
5514.709	-86:	0.50	
5517.659	-117	0.05	
5517.674	-127	0.07	
5519.670	-83	0.82	
5519.6855	-78	0.85	
RW CNC	(2439556.314,	0.547199)	
5357.8405	-79	0.22	
5357.8545	-75	0.25	
5359.842	-93	0.88	
5359.856	-97	0.91	
5361.841	-68	0.54	
5361.856	-64	0.56	
SS CNC	(2423078.589,	0.36733792)	
5358.754	-22	0.05	
5358.7715	-50	0.10	
TT CNC	(2439944.367,	0.5634494)	
5272.992	24	0.15	
5273.006	31	0.17	
5358.8085	46	0.45	
5358.821	30	0.48	
5359.8045	12	0.22	

TABLE II (Continued)

HJD (2440000+)	V_r (km/sec)	PHASE
5359.8185	27	0.25
5361.752	51	0.68
5361.766	63	0.70
RV CET (2439113.363, 0.623403)		
5273.8035	-95	0.96
5273.821	-108	0.98
S COM (2440654.641, 0.5865907)		
5359.9755	-57	0.50
5359.9895	-41	0.52
5360.9665	-75	0.18
5360.9805	-57	0.21
5361.967	-32	0.89
5361.981	-80	0.91
ST COM (2427862.585, 0.5989295)		
5357.035	-75	0.53
5358.025	-91	0.18
5358.039	-85	0.21
5362.0075	-51	0.83
5362.0215	-58	0.86
5457.761	-56	0.71
5457.778	-24	0.74
RV CRB (2441451.413, 0.331619)		
5457.885	-131	0.55
5457.9025	-138	0.60
5460.9435	-111	0.77
5460.956	-107	0.81
5514.777	-137	0.11
5514.7905	-126	0.15
5518.8145	-133	0.29
5518.830	-144	0.33
X CRT (2427858.345, 0.73283324)		
5458.697	104	0.86
5458.712	100	0.88
5459.729	69	0.27
5459.743	64	0.29
5460.6825	99	0.57
5460.6965	87	0.59
Z CVN (2438931.371, 0.653819)		
5460.721	29	0.48
5460.7345	15	0.50
5462.6765	7	0.47
5462.690	14	0.49
RZ CVN (2437823.433, 0.5674174)		
5459.7675	-11	0.05
5459.7815	-14:	0.08
5460.7605	-43	0.80
5460.7745	-40	0.83
5461.788	-7	0.62
5461.802	-1:	0.64

TABLE II (Continued)

HJD (2440000+)	V_r (km/sec)	PHASE
ST CVN (2436400.350, 0.32906263)		
5459.8035	-135	0.09
5459.8175	-113	0.13
5515.666	-130	0.85
5515.6815	-114	0.90
XZ CYG (2441453.386, 0.4664731)		
5269.636	-132	0.07
5269.647	-136	0.10
UY CYG (2422433.727, 0.56070478)		
5518.856	39	0.63
5518.871	28	0.66
5519.902	3	0.49
5519.916	2	0.52
DX DEL (2430950.506, 0.47261673)		
5226.7525	-15	0.82
5226.763	-16	0.84
SW DRA (2426224.5876, 0.56966993)		
5448.653	-34	0.98 (rvm)
5449.649	-13	0.72 (rvm)
RR GEM (2439098.886, 0.3973158)		
5268.972	82	0.43
5268.9835	78	0.46
5273.976	42	0.02
5273.997	44	0.07
5361.7145	22	0.85
5361.7285	24	0.88
SZ GEM (2433737.364, 0.50113615)		
5357.788	298	0.16
5357.805	311	0.19
VZ HER (2436788.898, 0.44032789)		
5458.880	-97	0.83
5458.894	-113	0.86
5459.9285	-119	0.21
5460.911	-110	0.44
5460.9235	-93	0.47
5515.789	-143	0.07
5515.803	-142	0.11
AR HER (2439692.681, 0.470025)		
5458.8425	-353	0.78
5458.858	-360	0.81
5460.8795	-333	0.11
5460.892	-340	0.14
5519.765	-332	0.39
5519.7805	-339	0.42
CE HER (2427861.668, 1.2094357)		
5514.831	-268	0.20

TABLE II (Continued)

HJD (2440000+)	V_r (km/sec)	PHASE	
5514.8465	-269	0.21	
5515.829	-244	0.02	
5515.8445	-291	0.04	
5516.7175	-237	0.76	
5516.735	-240	0.77	
5518.7735	-236:	0.46	
5518.789	-243	0.47	
SZ HYA (2440679.412, 0.53724022)			
5361.803	137	0.64	
5361.817	157	0.66	
WZ HYA (2436613.445, 0.5377229)			
5361.8775	287	0.41	
5361.8915	288	0.43	
5459.652	286	0.24	
5459.6655	286	0.26	
5461.643	332	0.94	
5461.657	324:	0.97	
RR LEO (2441736.450, 0.4523896)			
5357.882	74	0.12	
5357.8925	79	0.14	
5358.925	77	0.42	
5358.9355	79	0.45	
5360.893	109	0.77	
5360.9055	106	0.80	
5444.665	109	0.95	(rvm)
5447.619	90	0.48	(rvm)
5447.715	108	0.69	(rvm)
5448.623	110	0.70	(rvm)
5449.760	75	0.21	(rvm)
RX LEO (2436306.383, 0.6534122)			
5358.9645	-153	0.32	
5358.9785	-130	0.34	
5361.927	-108	0.85	
5361.944	-104	0.88	
5461.7185	-103	0.58	
5461.732	-112	0.60	
5462.642	-131	0.99	
5462.656	-147	0.01	
SS LEO (2427966.765, 0.62634289)			
5356.9795	188	0.69	
5359.006	205	0.92	
5457.6885	175	0.48	
5457.706	176	0.50	
5460.647	148	0.20	
5460.661	140	0.22	
SZ LEO (2425331.400, 0.5340833)			
5358.9045	174	0.84	
5458.654	200:	0.61	
5458.6715	194	0.64	

TABLE II (Continued)

HJD (2440000+)	V_r (km/sec)	PHASE
5459.6895	199	0.55
5459.703	187	0.57
5461.682	212	0.28
5461.697	194	0.31
TV LEO (2439216.712, 0.672843)		
5359.9335	-112	0.25
5359.9475	-107	0.27
5360.930	-75	0.73
5360.944	-79	0.75
V LMI (2419530.341, 0.5439187)		
5357.9265	-119	0.28
5357.9405	-136	0.30
5359.8855	-93	0.88
5359.899	-95	0.90
5360.854	-92	0.66
5360.8715	-114	0.69
TV LYN (2440950.922, 0.240651)		
5271.955	17	0.60
5271.9905	-3	0.75
RR LYR (2438215.377, 0.56683)		
5269.5875	-37	0.02
5269.591	-34	0.03
ST OPH (2418159.662, 0.45035643)		
5458.9285	7	0.02
5458.9445	-21	0.06
5516.7695	9	0.46
5516.785	5	0.49
5517.817	52	0.78
5517.8345	13	0.82
VV PEG (2438728.689, 0.4883847)		
5514.9155	-1:	0.25
5514.9305	7	0.28
5517.9385	38	0.44
5517.9525	25	0.47
5519.941	11	0.54
5519.956	16	0.57
CG PEG (2439712.949, 0.4671385)		
5272.6715	16	0.66
5272.6925	13	0.70
5518.9395	35	0.84
5518.9535	37	0.87
TU PER (2438772.590, 0.60707)		
5360.5825	-331	0.11
AR PER (2438729.726, 0.4255494)		
5270.9595	2	0.27
5270.971	6	0.29
5272.8955	24	0.82

TABLE II (Continued)

HJD (2440000+)	V_r (km/sec)	PHASE
5272.907	23	0.84
5355.801	5	0.64
5355.8145	19	0.67
5357.7135	-27	0.13
5357.724	-21	0.16
5360.620	19	0.96
5360.6325	-8	0.99
5361.6345	-30	0.34
5361.6485	-22	0.38
RU PSC (2424057.945, 0.3903174)		
5226.9375	-116	0.33
5226.955	-133	0.37
SS PSC (2428241.482, 0.2877924)		
5270.800	-14	0.23
5270.823	-11	0.31
XX PUP (2438809.690, 0.51719805)		
5360.7475	358	0.44
5360.7615	366	0.47
BB PUP (2438810.771, 0.4799387)		
5360.798	94	0.63
5360.8155	95	0.67
RU SCL (2438339.402, 0.4933333)		
5272.7295	58	0.04
5272.741	61	0.07
AN SER (2414708.950, 0.52207162)		
5446.952	-76	0.99 (rvm)
5448.772	-45	0.47 (rvm)
5448.904	-27	0.72 (rvm)
5449.744	-50	0.33 (rvm)
AR SER (2442206.390, 0.575109)		
5446.936	113	0.66 (rvm)
5459.886	110	0.18
5459.8985	117	0.20
5514.738	133	0.56
5514.752	136	0.58
5517.772	155	0.83
5517.7875	173	0.86
5518.673	107	0.40
5518.6885	107	0.43
AT SER (2428343.221, 0.7465682)		
5518.7365	-46	0.96
5519.728	-73	0.28
5519.743	-61	0.30
SS TAU (2437960.419, 0.3699186)		
5273.914	-11	0.55
5273.949	-28	0.65

TABLE II (Continued)

HJD (2440000+)	V_r (km/sec)	PHASE
UV VIR (2426126.412, 0.5870824)		
5357.977	115	0.86
5357.9945	121	0.89
AV VIR (2427871.614, 0.656908)		
5360.014	135	0.30
5360.028	131	0.32
5361.0065	176	0.81
5361.0205	178	0.83
5458.7405	174	0.59
5458.7575	177	0.61
5461.7555	124	0.18
5461.769	124	0.20
BN VUL (2434244.333, 0.59412538)		
5272.5735	-284	0.14
5514.875	-248	0.97
5514.8885	-241	0.00
5515.8655	-258	0.64
5515.879	-250	0.66
5519.8215	-296	0.30
5519.8355	-295	0.32

telescope (denoted by "rvm"). This instrument and its data-reduction procedure have been described in detail in Slovak, van Citters, and Barnes (1979); our procedure was similar to theirs. Since the radial-velocity meter could be used only for the bright RR Lyrae stars with relatively strong metal lines and velocities in the range of -100 km sec^{-1} to $+100$ km sec^{-1}, it was of limited value to this particular program.

To compare the velocities obtained by the Cassegrain spectrograph and the radial-velocity meter, we observed the star RR Leonis several times with both instruments. Figure 1 shows that the two methods give excellent agreement.

IV. Mean Velocities

We were able to determine new mean velocities for 46 of the RR Lyrae stars in Table II. Three methods were employed. First, we found the arithmetic mean of our velocities and all previously published velocities. This mean is a fair approximation to the true mean velocity if there are several observations and if they are scattered randomly over the pulsation cycle. Because most RR Lyraes have slowly varying periods, it was impossible to phase the old observations with our data. Therefore this mean is our best estimate of the mean velocity for stars when our data alone are insufficient to fit a curve.

In the second method, a standard radial-velocity curve was fit to those stars which we had observed at three or

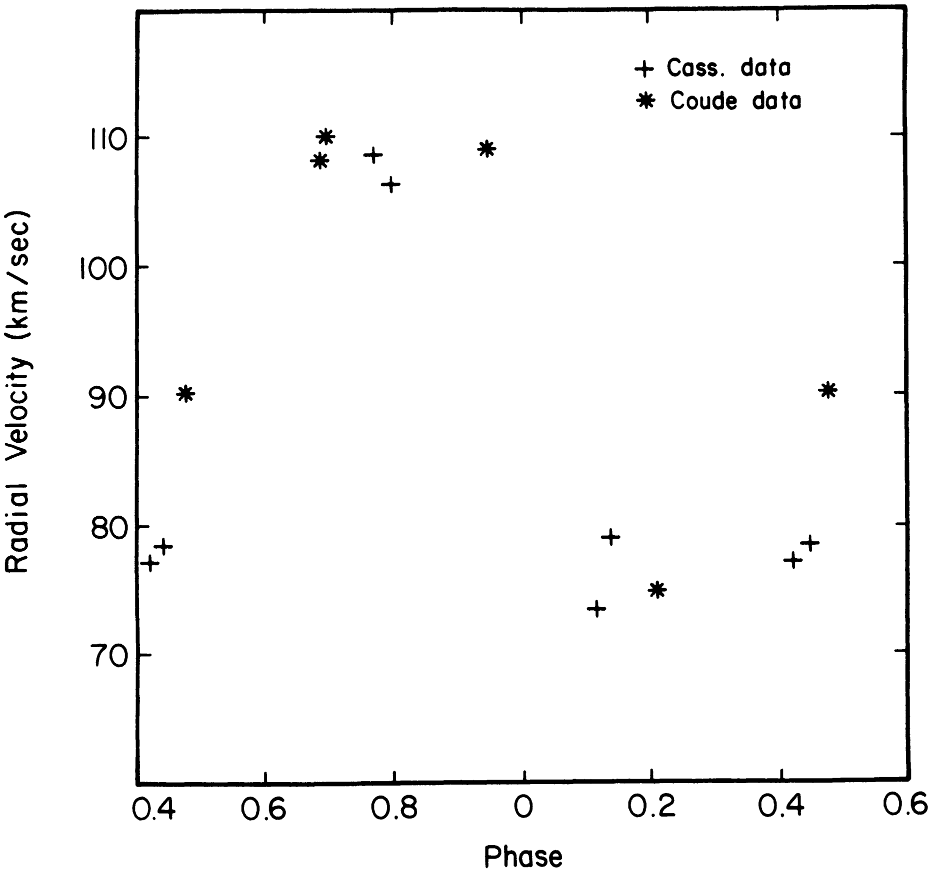

FIG. 1—Radial velocity vs. phase for RR Leo data taken with the Cassegrain spectrograph and the coudé radial-velocity meter. Good agreement is found between the two sets of velocities.

more distinct phases (observations from slit 1 and slit 2, typically less than 0.05 in phase apart, were not considered distinct in this sense). The standard radial-velocity curve was determined from an extensive set of observations of the RRab star X Arietis (Oke 1966). A least-squares fit of three line segments to his data gave a satisfactory standard curve, shown in Figure 2.

We fit this standard curve to our data using a geometric minimization technique known as simplex optimization to minimize, in a least-squares sense, the error in the residuals from the fit. (The technique of simplex optimization is discussed at length in Hawley et al. 1985). The free parameters in the fit were the epoch of maximum radial velocity and the mean radial velocity. Although RR Lyrae stars have amplitudes ranging from about 40 to 80 km sec^{-1}, the accuracy and number of our data did not warrant including the amplitude as a parameter in the analytic fit. To test the sensitivity of the analytic fit to the assumed amplitude and curve shape, we fit the RRab curve to two c-type stars, TV Bootis and RV Coronae Borealis. Since c-type variables are observed to have smaller amplitude, symmetric radial-velocity curves, this served as a test of the effect of the assumed radial-velocity curve characteristics on the derived mean velocity. Good agreement was found between the velocities from the three different methods for these two stars, indicating that the assumed amplitude should not have a large effect on the mean velocities.

Finally, the standard radial-velocity curve was subjectively applied to the data, with the goodness of fit being judged by eye. This method was used as a check on the other two, to ensure that no gross errors were being made as a result of poor sampling across the pulsation cycle.

Table III gives the new mean velocities we have determined and an estimate of the uncertainty in these values. The value previously published in the literature is included for comparison (Hemenway 1975, and references therein). The accuracy of our data and the fact that only a few observations of each star were obtained made assignment of a precise uncertainty inappropriate. We chose instead to place each star in one of three uncertainty classes. Uncertainty classes 1, 2, and 3 correspond to uncertainties of less than $\pm$ 5 km sec^{-1}, between $\pm$ 5 and $\pm$ 10 km sec^{-1} and greater than $\pm$ 10 km sec^{-1}, respectively. For two of the stars in Table III (SZ Leo and AV Vir), our mean radial velocity differs from the previously published value by nearly 100 km sec^{-1} or more. It is unlikely that the pulsation effect could lead to an error of

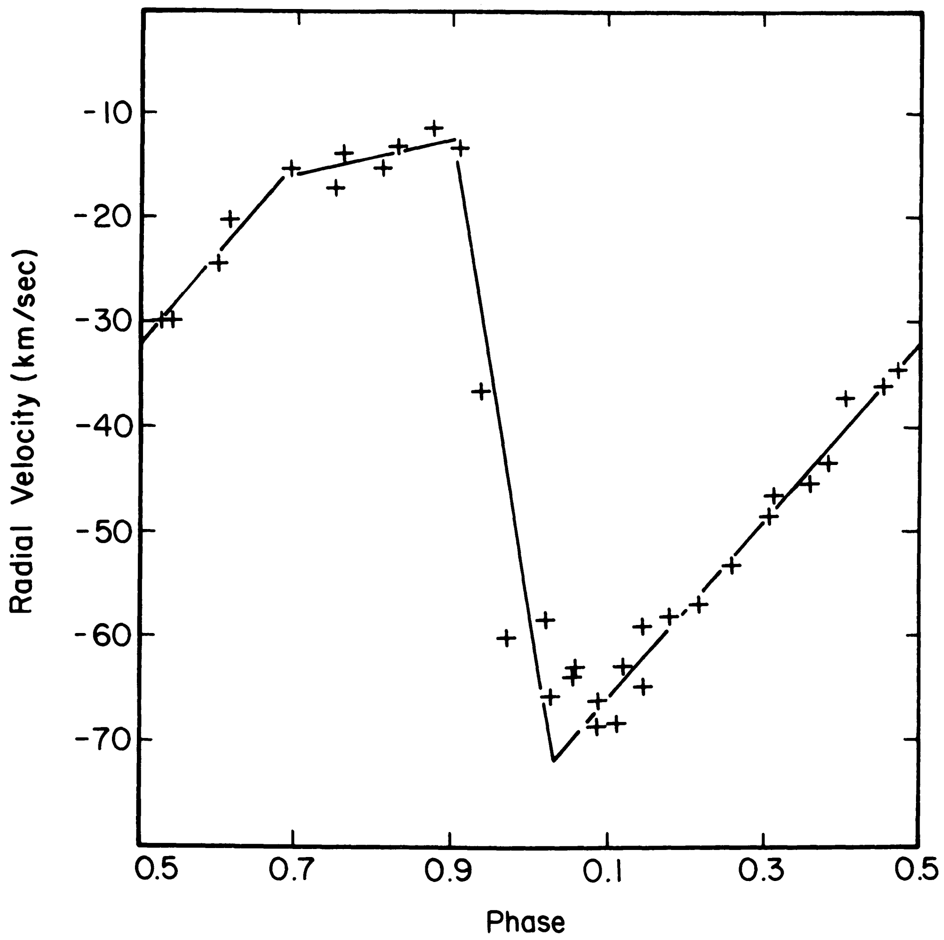

FIG. 2—Radial velocity vs. phase for X Ari data taken from Oke (1966). Three line segments were fit to the data to form a standard radial-velocity curve.

this magnitude. However, because we have several independent determinations of the radial velocity for each of these stars, we feel that our values are more likely to be the correct ones. It is possible that the previous investigators misidentified the stars, or had large errors in their radial-velocity determinations. For all of the stars in Table III, our newly obtained velocities significantly improved the determination of the mean radial velocity.

V. Conclusion

Radial-velocity observations of 57 field RR Lyrae stars have been made using a Cassegrain spectrograph on the 2.1-m telescope at McDonald Observatory. New mean radial velocities were determined for 46 of the stars. These velocities are now available for a new statistical analysis of the absolute magnitude and kinematic properties of the RR Lyrae stars.

This work was supported by NSF grant INT 81-17487 (T.G.B.). One of us (S.L.H.) gratefully acknowledges the support of McDonald Observatory and a ZONTA Amelia Earhart Fellowship. We would also like to thank Wan Lai, Frederic V. Hessman, and William H. Jefferys for their help throughout the course of this project.

REFERENCES

Fletcher, J. M., Harris, H. C., McClure, R. D., and Scarfe, C. D. 1982, *Pub. A.S.P.* **94**, 1017.

Hawley, S. L., Jefferys, W. H., Barnes, T. G., and Wan, L. 1985 (in preparation).

Hemenway, M. K. 1975, *A.J.* **80**, 199.

Hessman, F. V., Robinson, E. L., Nather, R. E., and Zhang, E.-H. 1984, *Ap. J.* **286**, 747.

Oke, J. B. 1966, *Ap. J.* **145**, 468.

Preston, G. W., and Paczynski, B. 1964, *Ap. J.* **140**, 181.

Slovak, M. H., van Citters, G. W., and Barnes III, T. G. 1979, *Pub. A.S.P.* **91**, 840.

Stothers, R. 1983, *Ap. J.* **274**, 20.

Stover, R. J., Robinson, E. L., Nather, R. E., and Montemayor, T. J. 1980, *Ap. J.* **240**, 597.

Vogt, S. S., Tull, R. G., and Kelton, P. 1978, *Appl. Opt.* **17**, 574.

Wan, L., Mao, Y-Q., and Ji, D-S. 1980, *Annals of Shanghai Observatory*, No. 2.

TABLE III

RR Lyrae Mean Radial Velocities

Name	Literature Mean Velocity	Our Mean Velocity	Uncertainty Class
AC AND	-69	-50	2
AT AND	-250	-240	3
SX AQR	-162	-178	3
AA AQL	-83	-30	1
V341 AQL	-135	-77	1
TZ AUR	30	45	2
ST BOO	21	14	1
TV BOO	-85	-64	1
TW BOO	-111	-99	1
RW CNC	-78	-86	2
TT CNC	49	49	2
Z CVN	0	20	3
RZ CVN	-15	-11	2
ST CVN	-85	-123	3
S COM	-34	-55	1
ST COM	-100	-68	2
RV CRB	-100	-125	1
X CRT	91	78	1
UY CYG	-5	3	2
SW DRA	-30	-33	3
RR GEM	94	60	1
SZ GEM	332	305	3
VZ HER	-120	-115	1
AR HER	-335	-350	2
CE HER	-235	-258	2
WZ HYA	315	304	2
RR LEO	65	94	1
RX LEO	-103	-127	2
SS LEO	145	180	2
SZ LEO	90	187	1
TV LEO	-95	-102	2
V LMI	-85	-110	2
TV LYN	-6	-7	2
ST OPH	-45	9	2
VV PEG	10	15	3
CG PEG	-10	2	2
TU PER	-380	-377	3
AR PER	-6	1	1
RU PSC	-131	-131	2
XX PUP	409	374	3
BB PUP	105	82	3
AN SER	-60	-47	1
AR SER	100	133	1
AT SER	-70	-55	3
AV VIR	35	154	1
BN VUL	-235	-267	1